The current issue and full text archive of this journal is available at
www.emeraldinsight.com/0961-5539.htm

Finite element modelling of the squeeze casting process

Eligiusz W. Postek
School of Engineering, University of Wales Swansea, Swansea, UK and
School of Earth and Environment, Institute of Geophysics and Techniques, University of Leeds, Leeds, UK, and
Roland W. Lewis and David T. Gethin
School of Engineering, University of Wales Swansea, Swansea, UK

Received 28 November 2006
Revised 25 May 2007
Accepted 25 May 2007

Abstract

Purpose – This paper sets out to present developments of a numerical model of squeeze casting process.

Design/methodology/approach – The entire process is modelled using the finite element method. The mould filling, associated thermal and thermomechanical equations are discretized using the Galerkin method. The front in the filling analysis is followed using volume of fluid method and the advection equation is discretized using the Taylor Galerkin method. The coupling between mould filling and the thermal problem is achieved by solving the thermal equation explicitly at the end of each time step of the Navier Stokes and advection equations, which allows one to consider the actual position of the front of the filling material. The thermomechanical problem is defined as elasto-visco-plastic described in a Lagrangian frame and is solved in the staggered mode. A parallel version of the thermomechanical program is presented. A microstructural solidification model is applied.

Findings – During mould filling a quasi-static Arbitrary Lagrangian Eulerian (ALE) is applied and the resulting temperatures distribution is used as the initial condition for the cooling phase. During mould filling the applied pressure can be used as a control for steering the distribution of the solidified fractions.

Practical implications – The presented model can be used in engineering practice. The industrial examples are shown.

Originality/value – The quasi-static ALE approach was found to be applicable to model the industrial SQC processes. It was found that the staggered scheme of the solution of the thermomechanical problem could parallelize using a multifrontal parallel solver.

Keywords Finite element analysis, Thermodynamics, Material-deforming processes

Paper type Research paper

1. Introduction

The paper deals with the presentation of developments of a squeeze casting model which has been developed, Lewis *et al.* (2006). The problem consists of two stages, namely, a mould filling simulation and thermal stresses analysis. Both stages include solidification. The flow problem is solved using the Galerkin method. The free surface

The authors would like to thank the Engineering and Physical Sciences Research Council (UK) and GKN Squeezeform (contract: GR/R80001/01) and EC – Research Infrastructure Action under the FP6 "Structuring the European Research Area" Programme HPC-Europa (contract: 506079).

International Journal of Numerical Methods for Heat & Fluid Flow
Vol. 18 No. 3/4, 2008
pp. 325-355

0961-5539
DOI 10.1108/09615530810853619

tracking problem is solved using a pseudo-concentration function method. The corresponding advection equation is discretized using a Taylor-Galerkin method. To solve the thermal problem the enthalpy method is applied. The thermomechanical problem is coupled and solved using a staggered scheme. The systems of linear equations appearing at each time step are solved using a parallel solver. An application of a microstructural solidification model is presented. Finally, the model is illustrated by solutions of a few industrial examples.

A general overview of squeeze casting processes with their classification is given by Ghomashi and Vikhrov (2000). A specific application of coupled thermomechanical problem to description of casting processes is given in the early work by Williams *et al.* (1979). A description of thermomechanical problems is shown by Sluzalec (1992), Vaz and Owen (1996) and Kleiber (1993). The solutions of flow problems are presented by Taylor and Hughes (1981), Zienkiewicz *et al.* (2005) and Donea and Huerta (2003). A model of mould filling using mixed Lagrangian-Eulerian technique is elaborated by Lewis *et al.* (1997). Methods of solving thermal problems including phase transformation are described by Lewis *et al.* (1996, 2004) and Celentano (2002). An interesting work about solution of a thermal problem using parallel techniques is presented by Masters *et al.* (1997).

2. Theoretical description

2.1 Thermal problem

Let us consider the heat transfer equation of the form:

$$\nabla(k\nabla T) + q = \rho c_{\mathrm{p}} \frac{\partial T}{\partial t} \quad \text{on} \quad \Omega \tag{1}$$

where k is the thermal conductivity, ∇T is the temperature gradient, q is the heat source, ρ is the mass density and c_{p} is the heat capacity. The equation is solved over the body Ω and fulfills the following Dirichlet and Neumann boundary conditions, respectively:

$$\begin{aligned} S_1(T) &= T - T_{\mathrm{w}} = 0 \ \text{ on } \ \partial\Omega_1 \\ S_2(T) &= k\left(\frac{\partial T}{\partial n}\right) + h(T - T_{\mathrm{w}}) \ \text{ on } \ \partial\Omega_2 \end{aligned} \tag{2}$$

where T_{w} is the temperature of the wall, h is the interfacial heat transfer coefficient and $\left(\partial T/\partial n\right)$ is the heat flux normal to the boundary. The boundary conditions are valid on the relevant boundaries $\partial\Omega_1$ and $\partial\Omega_2$, respectively. Assuming the approximation of the temperature field:

$$\mathbf{T} = \mathbf{N}\mathbf{T}_{\mathrm{q}} \tag{3}$$

where $\mathbf{N}$ is the shape functions matrix and $\mathbf{T}_{\mathrm{q}}$ is the vector of the nodal temperatures, then, performing the Galerkin method we obtain the discretized form of equations (1) and (2):

$$\mathbf{K}\mathbf{T} + \mathbf{C}\dot{\boldsymbol{T}} = \dot{\boldsymbol{F}} \tag{4}$$

where $\mathbf{K}$, $\mathbf{C}$ are the conductivity and heat capacity matrices, respectively, and $\mathbf{F}$ is the thermal loading vector. These are defined as follows:

$$K_{ij} = \int_{\Omega} \nabla N_i k \nabla N_j \mathrm{d}\Omega + \int_{\partial\Omega_3} N_i h N_j \mathrm{d}(\partial\Omega) - \int_{\partial\Omega_1} N_i k \frac{\partial N_j}{\partial n} \mathrm{d}(\partial\Omega),$$
$$C_{ij} = \int_{\Omega} N_i c_p \rho N_j \mathrm{d}\Omega, \tag{5}$$
$$F_i = \int_{\Omega} N_i q \mathrm{d}\Omega + \int_{\partial\Omega_3} N_i h T_{\mathrm{w}} \mathrm{d}(\partial\Omega)$$

Equation can be solved using either implicit or explicit time marching schemes. In our case an implicit scheme has been chosen.

In the case of phase transformation, due to the existence of a strong discontinuity in the dependence of heat capacity with respect to time, the enthalpy method is applied, Morgan *et al.* (1978), McAdie *et al.* (1995), Celentano and Perez (1996) and Lewis *et al.* (2004). The main idea of the enthalpy method is the involvement of a new variable (enthalpy). This allows us to regularize the sharp change in heat capacity due to the release of latent heat during the phase transformation and leads to a faster convergence. The enthalpy formulation of equation (4) is given as follows:

$$\mathbf{K}\mathbf{T}_N + \frac{\mathrm{d}\mathbf{H}}{\mathrm{d}T}\dot{\boldsymbol{T}}_N = \mathbf{F} \tag{6}$$

The definitions of the enthalpy variable for pure metals and alloys are given by equation (7) as follows:

$$H = \begin{cases} \int_0^{T_{\mathrm{m}}} c \mathrm{d}T, & T \le T_{\mathrm{m}} \\ \int_0^{T_{\mathrm{m}}} c \mathrm{d}T + (1 - f_{\mathrm{s}})\Delta h_f & T = T_{\mathrm{m}} \\ \int_0^{T_{\mathrm{end}}} c \mathrm{d}T + \Delta h_{\mathrm{f}}, & T > T_{\mathrm{m}} \end{cases}$$

$$H = \begin{cases} \int_0^{T_{\mathrm{sol}}} c \mathrm{d}T, & T \le T_{\mathrm{sol}} \\ \int_0^{T_{\mathrm{liq}}} c \mathrm{d}T + (1 - f_{\mathrm{s}})\Delta h_{\mathrm{f}}, & T_{\mathrm{sol}} \le T \le T_{\mathrm{liq}} \\ \int_0^{T_{\mathrm{end}}} c \mathrm{d}T + \Delta h_{\mathrm{f}}, & T > T_{\mathrm{liq}} \end{cases} \tag{7}$$

where T_{m} is the metal melting temperature, T_{sol}, T_{liq} are the temperatures of the solid and liquid phases, respectively, f_{s} is the amount of solid fraction (volume), Δh_{f} is the latent heat and T_{end} is the temperature at the end of the process.

The following averaging formula, Morgan *et al.* (1978) was used for the estimation of the enthalpy variable:

$$(\rho c_p) \cong \left(\frac{(\partial H/\partial x)^2 + (\partial H/\partial y)^2 + (\partial H/\partial z)^2}{(\partial T/\partial x)^2 + (\partial T/\partial y)^2 + (\partial T/\partial z)^2} \right)^{1/2} \tag{8}$$

The same formula was also used in the case of the mould filling and thermal stresses analyses. The thermal equation is integrated explicitly in the case of mould filling analysis while implicit scheme has been chosen for the case of the thermal stresses analysis.

2.2 Mechanical problem

The mechanical problem is initially treated as elasto-viscoplastic in nature with the assumption of large displacements, Zienkiewicz and Taylor (2005), Bathe (1996) and Kleiber (1989). Further, we will include the finite strains effect. The total potential energy is of the form:

$$\Pi = \int_{\Omega^o} \frac{1}{2} {}^{t+\Delta t}_{o}\mathbf{S} \cdot {}^{t+\Delta t}_{o}\mathbf{E} \mathrm{d}\Omega^o - \int_{\Omega^o} {}^{t+\Delta t}\mathbf{f}^{t+\Delta t}\mathbf{u} \mathrm{d}\Omega^o - \int_{\partial\Omega^t_\sigma} {}^{t+\Delta t}\mathbf{t}^{t+\Delta t}\mathbf{u} \mathrm{d}\left(\partial\Omega^t_\sigma\right) \tag{9}$$

where $\mathbf{S}$ and $\mathbf{E}$ are the II Piola-Kirchhof stress tensor and the Green Lagrange strains, $\mathbf{f}$, $\mathbf{t}$ and $\mathbf{u} = \{u,v,w\}$ are the body forces, boundary tractions and displacements. All the quantities are determined at time $t + \Delta t$ in the initial configuration, "o". By taking the variation of equation (9) we obtain the virtual work equation of the form:

$$\delta\Pi = \int_{\Omega^o} {}^{t+\Delta t}_{o}\mathbf{S} \cdot \delta {}^{t+\Delta t}_{o}\mathbf{E} \mathrm{d}\Omega^o - \int_{\Omega^o} {}^{t+\Delta t}\mathbf{f}\delta^{t+\Delta t}\mathbf{u} \mathrm{d}\Omega^o - \int_{\partial\Omega^o_\sigma} {}^{t+\Delta t}\mathbf{t}\delta^{t+\Delta t}\mathbf{u} \mathrm{d}\left(\partial\Omega^o_\sigma\right) \tag{10}$$

Exploiting the following relations, Malvern (1969) and Crisfield (1997):

$${}^{t+\Delta t}_{o}\mathbf{S} = \frac{\rho}{\rho_o} {}^{t+\Delta t}_{t}\mathbf{S}, \quad {}^{t+\Delta t}_{o}\mathbf{E} = \frac{\rho}{\rho_o} {}^{t+\Delta t}_{t}\mathbf{E}, \rho \mathrm{d}\Omega^t = \rho_o \mathrm{d}\Omega^o \tag{11}$$

we obtain the above virtual equation:

$$\int_{\Omega^t} {}^{t+\Delta t}_{t}\mathbf{S} \cdot \delta {}^{t+\Delta t}_{t}\mathbf{E} \mathrm{d}\Omega^t = \int_{\Omega^t} {}^{t+\Delta t}\mathbf{t}\delta^{t+\Delta t}\mathbf{u} \mathrm{d}\Omega^t + \int_{\partial\Omega^t_\sigma} {}^{t+\Delta t}\mathbf{t}\delta^{t+\Delta t}\mathbf{u} \mathrm{d}\left(\partial\Omega^t_\sigma\right) \tag{12}$$

Now, the goal becomes one of obtaining the final form of the virtual work equation before discretization. To achieve this the following incremental decomposition is employed:

$$\begin{aligned}
{}^{t+\Delta t}_{t}\mathbf{E} &= {}^{t}_{t}\mathbf{E} + \Delta\mathbf{E}, \\
{}^{t+\Delta t}_{t}\mathbf{S} &= {}^{t}_{t}\mathbf{S} + \Delta\mathbf{S}, \\
{}^{t+\Delta t}\mathbf{u} &= {}^{t}\,\mathbf{u} + \Delta\mathbf{u}, \\
{}^{t+\Delta t}\mathbf{f} &= {}^{t}\,\mathbf{f} + \Delta\mathbf{S}, \\
{}^{t+\Delta t}\mathbf{t} &= {}^{t}\,\mathbf{t} + \Delta\mathbf{t}
\end{aligned} \tag{13}$$

along with the following relations for stress increments (${}^{t}_{t}\boldsymbol{\tau}$ is the Cauchy stress tensor):

$$\begin{aligned}
{}^{t}_{t}\mathbf{S} &= {}^{t}_{t}\boldsymbol{\tau}, \\
{}^{t+\Delta t}_{t}\mathbf{S} &= {}^{t}_{t}\boldsymbol{\tau} + \Delta\mathbf{S}, \\
\Delta\mathbf{E} &= \Delta\mathbf{e} + \Delta\boldsymbol{\eta}, \\
\Delta\mathbf{e} &= \bar{\mathbf{A}}\Delta\mathbf{u}, \\
\Delta\boldsymbol{\eta} &= \frac{1}{2}\bar{\bar{\mathbf{A}}}(\Delta\mathbf{u}')\Delta\mathbf{u}'
\end{aligned} \tag{14}$$

and also the following strain increment decomposition into its linear and nonlinear parts where $\Delta\mathbf{u}'$ is the vector of the displacement increment derivatives w.r.t. Cartesian coordinates and $\bar{\mathbf{A}}$, $\bar{\bar{\mathbf{A}}}$ are the linear and non-linear operators as follows:

$$\overline{\mathbf{A}} = \begin{bmatrix} \frac{\partial}{\partial x} & 0 & 0 \\ 0 & \frac{\partial}{\partial y} & 0 \\ 0 & 0 & \frac{\partial}{\partial z} \\ \frac{\partial}{\partial y} & \frac{\partial}{\partial x} & 0 \\ \frac{\partial}{\partial z} & 0 & \frac{\partial}{\partial x} \\ 0 & \frac{\partial}{\partial z} & \frac{\partial}{\partial y} \end{bmatrix}$$

$$\bar{\bar{\mathbf{A}}} = \begin{bmatrix} \Delta u_{,x} & 0 & 0 & \Delta v_{,x} & 0 & 0 & \Delta w_{,x} & 0 & 0 \\ 0 & \Delta u_{,y} & 0 & 0 & \Delta v_{,y} & 0 & 0 & \Delta w_{,y} & 0 \\ 0 & 0 & \Delta u_{,z} & 0 & 0 & \Delta v_{,z} & 0 & 0 & \Delta w_{,z} \\ \Delta u_{,y} & \Delta u_{,x} & 0 & \Delta v_{,y} & \Delta v_{,x} & 0 & \Delta w_{,y} & \Delta w_{,x} & 0 \\ 0 & \Delta u_{,z} & \Delta u_{,y} & 0 & \Delta v_{,z} & \Delta v_{,y} & 0 & \Delta w_{,z} & \Delta w_{,y} \\ \Delta u_{,z} & 0 & \Delta u_{,x} & \Delta v_{,z} & 0 & \Delta v_{,x} & \Delta w_{,z} & 0 & \Delta w_{,x} \end{bmatrix} \tag{15}$$

Substituting the relations, equations (13-15), into the virtual work equation, equation (12) we arrive at:

$$\int_{\Omega^t} \left({}^t_t\boldsymbol{\tau} \cdot \delta\boldsymbol{\eta} + \Delta\mathbf{S} \cdot \delta\Delta\mathbf{e}\right) \mathrm{d}\Omega^t = \int_{\Omega^t} {}^{t+\Delta t}\mathbf{f}\delta^{t+\Delta t}\mathbf{u}\mathrm{d}\Omega^t + \int_{\partial\Omega^t_\sigma} {}^{t+\Delta t}\mathbf{t}\delta^{t+\Delta t}\mathbf{u}\mathrm{d}\left(\partial\Omega^t_\sigma\right) - \int_{\Omega^t} {}^t_t\boldsymbol{\tau} \cdot \delta\Delta\mathbf{e}\mathrm{d}\Omega^t \tag{16}$$

Equation (16) must be solved iteratively, however, for brevity we assume that the equation is fulfilled precisely at time t, as a result we obtain the following incremental form of the virtual work equation:

$$\int_{\Omega^t} \left({}^t_t\boldsymbol{\tau} \cdot \delta\boldsymbol{\eta} + \Delta\mathbf{S} \cdot \delta\Delta\mathbf{e}\right) \mathrm{d}\Omega^t = \int_{\Omega^t} \Delta\mathbf{f}\delta\Delta\mathbf{u}\mathrm{d}\Omega^t + \int_{\partial\Omega^t_\sigma} \Delta\mathbf{t}\delta\Delta\mathbf{u}\mathrm{d}\left(\partial\Omega^t_\sigma\right) \tag{17}$$

Employing the finite element approximation:

$$\Delta\mathbf{u} = \mathbf{N}\Delta\mathbf{q}, \quad \Delta\mathbf{u}' = \mathbf{B}'_{\mathrm{L}}\Delta\mathbf{q} \tag{18}$$

where $\mathbf{N}$ is the set of shape functions, $\Delta\mathbf{q}$ is the increment of nodal displacements and considering the following set of equalities:

$${}^t_t\boldsymbol{\tau}^T\delta\boldsymbol{\eta} = {}^t_t\boldsymbol{\tau}^T\delta(\bar{\bar{\mathbf{A}}})\Delta\mathbf{u}' = \delta(\Delta\mathbf{u}')^T{}^t_t\bar{\boldsymbol{\tau}}^{\mathrm{T}}\Delta\mathbf{u}' = \delta(\Delta\mathbf{q})^T{}^t_t\bar{\boldsymbol{\tau}}\mathbf{B}'_{\mathrm{L}} \tag{19}$$

where ${}^t_t\bar{\boldsymbol{\tau}}$ is the Cauchy stress matrix:

$$ {}^t_t\bar{\boldsymbol{\tau}} = \begin{bmatrix} {}^t_t\underline{\boldsymbol{\tau}} & & \\ & {}^t_t\underline{\boldsymbol{\tau}} & \\ & & {}^t_t\underline{\boldsymbol{\tau}} \end{bmatrix} \quad {}^t_t\underline{\boldsymbol{\tau}} = \begin{bmatrix} {}^t_t\sigma_{xx} & {}^t_t\tau_{xy} & {}^t_t\tau_{xz} \\ & {}^t_t\sigma_{yy} & \tau_{yz} \\ & & {}^t_t\sigma_{zz} \end{bmatrix} \tag{20} $$

we obtain the following discretized form of the virtual work equation:

$$ \left(\int_{\Omega^t} \mathbf{B}'^{\mathrm{T}}_{\mathrm{L}} {}^t_t\bar{\boldsymbol{\tau}} \mathbf{B}'_{\mathrm{L}} \mathrm{d}\Omega^t \right) \Delta\mathbf{q} + \int_{\Omega^t} \mathbf{B}^T_{\mathrm{L}} \Delta\mathbf{S} \mathrm{d}\Omega^t = \int_{\Omega^t} \mathbf{N}^T \Delta\mathbf{f} \mathrm{d}\Omega^t + \int_{\partial\Omega^t_\sigma} \mathbf{N}^T \Delta\mathbf{t} \mathrm{d}\left(\partial\Omega^t_\sigma\right) \tag{21} $$

where $\mathbf{B}'_L$ is the large displacements operator, $\mathbf{B}_{\mathrm{L}}$ is the linear operator, ${}^t_t\bar{\boldsymbol{\tau}}$ is the Cauchy stress matrix, $\mathbf{N}$ is the shape functions matrix, $\Delta\mathbf{q}$ is the displacements increment vector, $\Delta\mathbf{f}$ is the body forces increment vector and $\Delta\mathbf{t}$ is the tractions external load increment vector.

2.3 Finite strains formulation

2.3.1 Kinematics. The kinematics of the finite strains has been well described, for example, by Peric *et al.* (1992), Crisfield (1997) and Bathe (1996). The material derivative of a displacement is of the form:

$$ \mathbf{v} = \frac{\partial \mathbf{x}}{\partial t} \tag{22} $$

When denoting the initial configuration as $\mathbf{X}$ and the current configuration as $\mathbf{x}$ the deformation gradient definition takes the form:

$$ \mathbf{F} = \frac{\partial \mathbf{x}}{\partial \mathbf{X}} \tag{23} $$

The gradient of the material derivative relates the deformation gradient and the gradient of the material derivative:

$$ \mathbf{L} = \frac{\partial \mathbf{v}}{\partial \mathbf{x}} = \frac{\partial \mathbf{v}}{\partial \mathbf{X}} \frac{\partial \mathbf{X}}{\partial \mathbf{x}} = \dot{\mathbf{F}}\mathbf{F}^{-1} \tag{24} $$

The gradient of the material derivative can be decomposed into $\mathbf{D}$ which is the rate of deformation tensor and $\mathbf{W}$ which is the spin rate:

$$ \mathbf{L} = \mathbf{D} + \mathbf{W} \tag{25} $$

The deformation gradient and the spin are defined as follows:

$$ \mathbf{D} = \frac{1}{2}\left(\mathbf{L} + \mathbf{L}^T\right), \quad \mathbf{W} = \frac{1}{2}\left(\mathbf{L} - \mathbf{L}^T\right) \tag{26} $$

Now, we will use the decomposition of the gradient $\mathbf{F} = \mathbf{VR} = \mathbf{RU}$ ($\mathbf{V}$ and $\mathbf{U}$ are the left and right stretch tensors, $\mathbf{R}$ is the rotation tensor):

$$\mathbf{L} = \dot{\mathbf{R}}\mathbf{R}^T + \mathbf{R}\dot{\mathbf{U}}\mathbf{U}^{-1}\mathbf{R}^T \tag{27}$$

The following relations are valid:

$$\dot{\mathbf{F}} = \mathbf{R}\dot{\mathbf{U}} + \dot{\mathbf{R}}\mathbf{U}, \quad \mathbf{F}^{-1} = (\mathbf{R}\mathbf{U})^{-1} = \mathbf{U}^{-1}\mathbf{R}^{-1} = \mathbf{U}^{-1}\mathbf{R}^T \tag{28}$$

The unrotated deformation strain rate is the symmetric part of the second part in $\mathbf{L}$:

$$\mathbf{d} = (\dot{\mathbf{U}}\mathbf{U}^{-1} + \mathbf{U}^{-1}\dot{\mathbf{U}}) \tag{29}$$

Exploiting the orthogonality condition:

$$\mathbf{R}\mathbf{R}^{\mathrm{T}} = 1, \quad (\dot{\mathbf{R}}^T\mathbf{R}) = 0, \quad \mathbf{R}^T\dot{\mathbf{R}} + \dot{\mathbf{R}}^T\mathbf{R} = 0 \tag{30}$$

the unrotated deformation rate takes the form:

$$\mathbf{d} = \mathbf{R}^T\mathbf{D}\mathbf{R} \tag{31}$$

The analogous relation to the above one is also valid for the Cauchy stresses (because of the conjugacy):

$$\boldsymbol{\sigma}^u = \mathbf{R}^{\mathrm{T}}\boldsymbol{\sigma}\mathbf{R} \tag{32}$$

where $\boldsymbol{\sigma}^u$ and $\boldsymbol{\sigma}$ are the unrotated Cauchy stress and the true Cauchy stress, respectively.

Now, we will use the multiplicative gradient decomposition into its elastic and plastic parts (Figure 1):

$$\mathbf{F} = \mathbf{F}^e\mathbf{F}^p \tag{33}$$

The decomposed gradient can be substituted into the deformation rate definition, equation (24) and with the assumption of small elastic strains we arrive at the approximate relation:

$$\mathbf{L} \approx \mathbf{L}^e + \mathbf{L}^p \tag{34}$$

which also leads to the approximate relation for the elastic and plastic deformation rates (additiveness of the elastic and plastic deformation rates):

$$\dot{\mathbf{D}} \approx \dot{\mathbf{D}}^e + \dot{\mathbf{D}}^p \tag{35}$$

Now, we may transform the deformation rate (equation (35)) to the unrotated configuration exploiting the relation, equation (31) using the rotation matrix:

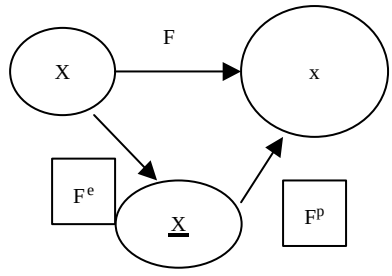

Figure 1.
Gradient decomposition

$$\mathbf{d} = \mathbf{R}^T(\mathbf{D}^e + \mathbf{D}^p)\mathbf{R} \tag{36}$$

which gives the elastic and plastic deformation rates additiveness in the unrotated configuration:

$$\mathbf{d} = \mathbf{d}^e + \mathbf{d}^p \tag{37}$$

The relation above and the relation for Cauchy stresses allows us to integrate the constitutive relations in the unrotated configuration as for small strains.

2.3.2 Stress updating procedure. To integrate the constitutive relations we exploit the relations given above using the integration for the unrotated configuration and the midpoint rule (Crank-Nicholson). The algorithm arises from relations (35) and (32). The outline of the integration scheme is given below:

(1) Compute deformation gradients:

$$\mathbf{F}^i_{t+\Delta t} = \frac{\partial\left(\mathbf{X} + \mathbf{u}^i_{n+1}\right)}{\partial \mathbf{X}}, \quad \mathbf{F}^i_{t+\Delta t/2} = \frac{\partial\left(\mathbf{X} + \mathbf{u}^i_{t+\Delta t/2}\right)}{\partial \mathbf{X}} \tag{38}$$

(2) Compute polar decompositions:

$$\mathbf{F}^i_{t+\Delta t} = \mathbf{R}^i_{t+\Delta t}\mathbf{U}^i_{t+\Delta t}, \quad \mathbf{F}^i_{t+\Delta t/2} = \mathbf{R}^i_{t+\Delta t/2}\mathbf{U}^i_{t+\Delta t/2} \tag{39}$$

(3) Compute deformation increment over the step:

$$\Delta\boldsymbol{\varepsilon}^i = \mathbf{B}^i_{t+\Delta t/2}\left(\mathbf{u}^i_{t+\Delta t} - \mathbf{u}_n\right) \tag{40}$$

(4) Now, we take the elements of the strain increment $\Delta\boldsymbol{\varepsilon}^{\mathrm{i}}$ and obtain the $\Delta\mathbf{D}^{\mathrm{i}}$ and perform rotation of the increment of spatial deformation to the unrotated configuration:

$$\Delta\mathbf{d}^i = \mathbf{R}^{i\mathrm{T}}_{t+\Delta t/2}\Delta\mathbf{D}^i\mathbf{R}^i_{t+\Delta t/2} \tag{41}$$

(5) Then, we perform integration of the small strains constitutive model using backward Euler integration rule (predictor-corrector):

$$\boldsymbol{\sigma}^{u(i)}_{t+\Delta t} = \boldsymbol{\sigma}^{u(i)}_{t+\Delta t}(\boldsymbol{\sigma}_t, \boldsymbol{\alpha}_t, \Delta\mathbf{d}^i) \tag{42}$$

Where the stresses depend on the history, this is reflected by the stresses at time t and internal parameters $\boldsymbol{\alpha}_t$.

(6) Transform the stresses to the true Cauchy stresses at $t + \Delta t$:

$$\boldsymbol{\sigma}_{t+\Delta t} = \mathbf{R}_{t+\Delta t}\boldsymbol{\sigma}^u_{t+\Delta t}\mathbf{R}^T_{t+\Delta t} \tag{43}$$

The integration in the unrotated configuration is performed using a consistent tangent formulation, Simo and Taylor (1985).

2.4 Microstructural solidification model

During the entire forming process a part of the solidification takes place. In order to describe the process more accurately a microstructure-based solidification model

has been employed. The model stems from the assumptions given by Celentano and Perez (1996). The basic assumptions are as follows: the sum of the solid and liquid fractions is equal one, the solid fraction consists of dendritic and eutectic fractions:

$$f_{\mathrm{l}} + f_{\mathrm{s}} = 1, \quad f_{\mathrm{s}} = f_{\mathrm{d}} + f_{\mathrm{e}} \tag{44}$$

Further assumptions are connected with the fact of the existence of interdendritic and intergranular eutectic fractions, the internal fraction consists of its dendritic and eutectic portions:

$$f_{\mathrm{s}} = f_g^{\mathrm{d}} f_i + f_g^{\mathrm{e}}, \quad f_i = f_i^{\mathrm{d}} + f_i^{\mathrm{e}} \tag{45}$$

The last assumptions lead to the final formulae for the dendritic and eutectic fractions (a spherical growth is assumed):

$$f_{\mathrm{d}} = f_g^{\mathrm{d}} f_i^{\mathrm{d}}, \quad f_{\mathrm{e}} = f_g^{\mathrm{d}} f_i^{\mathrm{e}} + f_g^{\mathrm{e}}, \quad f_g^{\mathrm{e}} = \frac{4}{3}\Pi N_{\mathrm{d}} R_{\mathrm{d}}^3, \quad f_i^{\mathrm{e}} = \frac{4}{3}\Pi N_{\mathrm{e}} R_{\mathrm{e}}^3 \tag{46}$$

N_{d}, N, N_{e} are the grain densities and R_{d}, R_{e} are the grain radii. The grain densities and grains sizes are governed by nucleation and growth evolution laws. The rate of growth of the dendritic and eutectic nuclei is given below. This depends on the undercooling and a Gaussian distribution of the nuclei is assumed:

$$\dot{N}_{(\mathrm{d,e})} = N_{\max(\mathrm{d,e})} \frac{1}{2\Pi} \exp\left(-\frac{\Delta T - \Delta T_{N(\mathrm{d,e})}}{2\Delta T_{\sigma(\mathrm{d,e})}}\right)\langle -\dot{T}\rangle, \quad \Delta T_{(\mathrm{d,e})} = T_{(\mathrm{d,e})} - T \tag{47}$$

The rate of the dendritic and eutectic grain radii is established based on experimental dependence:

$$\dot{R}_{(\mathrm{d,e})} = f_{R(\mathrm{d,e})} \tag{48}$$

Finally, the internal dendritic fraction depends on the melting temperature and k' is the partition coefficient:

$$f_i^{\mathrm{d}} = 1 - \left(\frac{T_{\mathrm{m}} - T}{T_{\mathrm{m}} - T_{\mathrm{l}}}\right)^{\frac{1}{k'-1}} \tag{49}$$

Two numerical examples concerning the mould filling and thermal stress development are provided.

2.5 Mould filling problem

The flow of material is assumed to be Newtonian and incompressible, Taylor and Hughes (1981), Ravindran and Lewis (1998) and Lewis and Ravindran (2000). The governing Navier Stokes equations are of the form:

$$\rho\left(\frac{\partial \mathbf{u}}{\partial t} + (\mathbf{u}\cdot\nabla)\mathbf{u}\right) = \nabla\cdot\mu\left[\nabla\mathbf{u} + (\nabla\mathbf{u})^T\right] - \nabla p + \rho\mathbf{g} \tag{50}$$

The mass conservation equation gives the incompressibility condition:

$$\nabla\cdot\mathbf{u} = 0 \tag{51}$$

where $\mathbf{u}$ is the velocity vector, p is pressure, μ is the dynamic viscosity and $\mathbf{g}$ is the gravitational acceleration vector. Performing the Galerkin procedure with a quadratic approximation for velocities $\mathbf{u} = \Sigma_i \mathbf{N}\mathbf{u}_n$ and linear approximation for pressures $\mathbf{p} = \Sigma_j \mathbf{N}'\mathbf{p}$ the discretized form of equations (50) and (51) is obtained:

$$\begin{bmatrix} \mathbf{M} & 0 \\ 0 & 0 \end{bmatrix} \begin{bmatrix} \frac{\mathbf{u}^{n+1}-\mathbf{u}^n}{\Delta t} \\ 0 \end{bmatrix} + \begin{bmatrix} \mathbf{K}_u & \mathbf{Q} \\ \mathbf{Q}^T & 0 \end{bmatrix} \begin{bmatrix} \mathbf{u}^{n+1} \\ \mathbf{p} \end{bmatrix} = \begin{bmatrix} \mathbf{f}_u \\ 0 \end{bmatrix} \tag{52}$$

where $\mathbf{M}$ is the mass matrix, $\mathbf{K}$ is the velocity stiffness matrix and $\mathbf{Q}$ is the divergence matrix. The r.h.s of equation (52) also contains external loading for the squeezed casting process.

To track the free surface the volume of fluid method is applied. Free surface tracking is governed by the first order advection equation:

$$\frac{\partial F}{\partial t} + (\mathbf{u} \cdot \nabla) F = 0 \tag{53}$$

where F is the pseudo-concentration function varying from -1 to 1, $F < 0$ indicates the empty region, $F > 0$ indicates the fluid region, $F = 0$ locates the free surface. The equation (53) is discretized with the Taylor-Galerkin method. An implicit time integration algorithm is used to solve the equation (52) and when considering the equation (53) an explicit integration scheme is used.

2.6 Thermal and mechanical contact

In our case the interfacial heat transfer coefficient is used for establishing the interface thermal properties of the layer between the mould and the cast part. The inclusion of this effect is critical in solidification processes because of the pressure and airgap effects. The interfacial heat transfer coefficient depends on the air conductivity k_{air}, thermal properties of the interfacing materials and the magnitude of the gap (g). The formula given by Lewis and Ransing (1998) and Ransing *et al.* (1999) is adopted:

$$h = \frac{k_{\text{air}}}{g + (k_{\text{air}}/h_o)} \tag{54}$$

The value of h_o, an initial heat transfer coefficient should be taken from experiment and reflects the influence of the type of interface materials where coatings may be applied. Additionally, from a numerical point of view, this allows us to regularize the dependence of the resulting interfacial coefficient on the gap magnitude. The dependence is also a source of coupling between the thermal and mechanical equations.

The basic assumption is that the whole cast part is in perfect contact with the mould at the beginning of the thermal stress analysis. The assumption is justified by the fact that the thermal stress analysis starts after the commencement of solidification. Because of the assumption concerning small deformations we may consider the so-called "node to node" approach in determining the contact characteristics. A penalty formulation is used which is briefly described. Considering the potential energy of an augmented mechanical system where, except for the standard stiffness matrix (linear or nonlinear) $\mathbf{K}$ and forces $\mathbf{F}$, there exists a system of constraints represented by the stiffnesses $\boldsymbol{\lambda}$. The constraints act between the contacting bodies. On calculating

the potential energy of the system, and then minimizing the energy, we arrive at an augmented system of equations taking into account the contact interactions:

$$\Pi = \frac{1}{2}\mathbf{q}^T\mathbf{K}\mathbf{q} - \mathbf{q}^T\mathbf{F} + \frac{1}{2}\mathbf{g}^T\boldsymbol{\lambda}\mathbf{g}, \quad \mathbf{K}'\mathbf{q} = \mathbf{F}' \tag{55}$$

The term $\mathbf{g}$ represents a vector of the penetration of contacting nodes into the contact surface and $\mathbf{K}'$ and $\mathbf{F}'$ are the augmented stiffness matrix and equivalent force vector, respectively. In the case of non-existence of the contact the distance between the nodes is calculated and in consequence the value is transferred to the thermal module where the interfacial heat transfer coefficient is calculated. The penalty number is an input data. In our implementation a possibility of keeping an assumed stiffness is kept even in the absence of contact between the nodes under consideration.

2.7 Coupling strategy, thermomechanical problem

Recalling the state equations of the thermal and mechanical problem in their discretized and abbreviated forms:

$$\begin{aligned} \mathbf{K}\mathbf{T}_n + \mathbf{C}\dot{\boldsymbol{T}}_n &= \mathbf{F}_T \\ \left(\mathbf{K}^{e-vp} + \mathbf{K}_g\right)\Delta\mathbf{q} &= \Delta\mathbf{Q} \end{aligned} \tag{56}$$

we may apply a staggered solution scheme, Felippa and Park (1980). The solution is obtained by sequential execution of the two modules (i.e. thermal and mechanical) (Figure 2).

The thermal problem is transient and nonlinear while the mechanical one is static and also nonlinear. The sources of nonlinearity in the static problem are the nonlinear and temperature dependent constitutive relations, nonlinear geometry and the contact relations. The sources of nonlinearity in the thermal problem are the temperature dependence of the conductivity and the heat capacity and the dependence of the interfacial heat transfer coefficient on the gap (equation (55)).

3. Parallel processing

We present the parallel application in the case of thermomechanical coupled problem (Postek *et al.*, 2005). Generally, the programming techniques for parallel models are

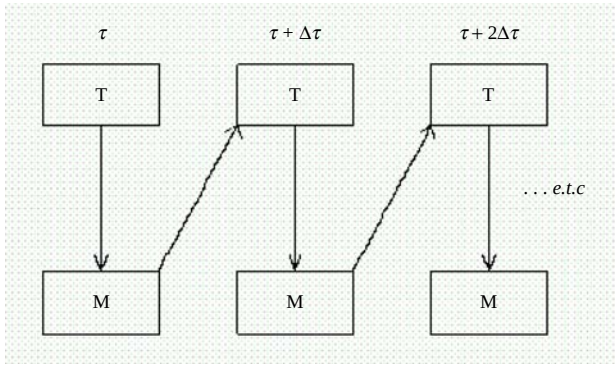

Note: Reproduced from the only available original

Figure 2.
Staggered scheme, thermomechanical problem

generally categorized by how memory is used and these can be divided into two categories:

(1) the "shared memory" model in which each processor accesses a shared memory space; and

(2) the "message passing model" in which each processor communicates with other processor by sending and receiving messages.

The message passing programming method is implemented on most parallel clusters by applying, e.g. the Message Passing Interface (Forum, MPI, 1994) library (1994). Computational tasks can reside on the same physical machine as well as across an arbitrary number of machines. The tasks exchange data through communications by sending and receiving messages. Data transfer usually requires that cooperative operations be performed by each processor. For example, a "send" operation must have a matching "receive" operation. The parallel implementation of the sequential code uses the message passing programming and is based on a domain decomposition. The sequential code is presented first then the parallel implementation, using the multifrontal parallel solver (MUMPS), Amestoy *et al.* (2000, 2001) working with MPI, is described.

3.1 Sequential code

The sequential code is written in Fortran 90 and contains two main modules:

(1) the mechanical module (denoted **M**) which solves the mechanical problem by using the Newton-Raphson method; and

(2) the thermal module (denoted **T**) which solves the thermal problem by using the Crank-Nicholson integration rule.

The two modules are both independently solved with a certain number of iterations. Data are transferred between these two modules at time step $t + \Delta t$. Algorithm (1) points out the main tasks of the sequential code.

Algorithm 1. Main tasks of the sequential code (staggered solution scheme):

```
1: t = 0
2: repeat
3:    {Thermal module}
4:    repeat
5:       Build the stiffness matrix and the right-hand side vector for the thermal
         module
6:       Crank Nicholson scheme
7:       Solve the linear system
8:    until converged
9:    {Mechanical module}
10:   repeat
11:      Build the stiffness matrix and the right-hand side vector for the mechanical
         module
12:      Newton-Raphson scheme
13:      Solve the linear system
14:   until converged
15:   Exchange data between the modules
16:   t + Δt
17: until t < total time
```

3.2 Parallel code using the MUMPS software

Following the above-staggered scheme a consistent parallelization algorithm is applied. The above-mentioned MUMPS solver takes as input parameters the linear systems and the number N of processors. It builds a partition with the METIS software, Karypis and Kumar (1997), of the linear system on each processor and solves it in parallel. The solver is also called in a staggered mode on using different partitions for the thermal and mechanical modules. Algorithm (2) describes the main tasks of the parallel code.

Algorithm 2. Main tasks of the parallel code (staggered solution scheme):

1: $t = 0$
2: repeat
3: {Thermal module}
4: repeat
5: Build the stiffness matrix and the right-hand side vector for the thermal module
6: Crank-Nicholson scheme
7: Solve the linear system in parallel on N processors by using MUMPS
8: **until** converged
9: {Mechanical module}
10: repeat
11: Build the stiffness matrix and the right-hand side vector for the mechanical module
12: Newton-Raphson scheme
13: Solve the linear system in parallel on N processors by using MUMPS
14: **until** converged
15: Exchange data between the two modules
16: $t + \Delta t$
17: **until** $t <$ total time

4. Numerical examples

4.1 Mould filling, valve

The numerical example concerns filling of a valve with aluminium alloy LM25. During the filling process solidification of the material is observed. The initial temperature of the cast is 650°C and initial temperature of the mould is 150°C. The ambient temperature is 20°C. The interfacial heat transfer coefficient is 6,000 $W/m^{2\circ}C$. The material density is 2,520 kg/m^3. The wall friction angle is 135°. The filling time is 10 s. The mould is made of steel H13. The cast and mould are discretized with 10,422 nodes and 4,917 elements. The discretization is shown in Figure 3. The microstructural data are shown in Figure 4(a)-(d), namely the dependences of heat capacity and conductivity on temperature and radius rates of the dendritic and eutectic grains. A qualitative difference is seen between Figures 5 to 10 where the temperatures distributions and the distributions of the dendritic and eutectic fractions are presented. This happened due to a much faster filling of the mould when the pressure was applied. The percentage of filling versus time dependency is shown in Figure 11. When the pressure is applied the filling time is 2.3 s while in the case of free filling the time is approximately 10 s.

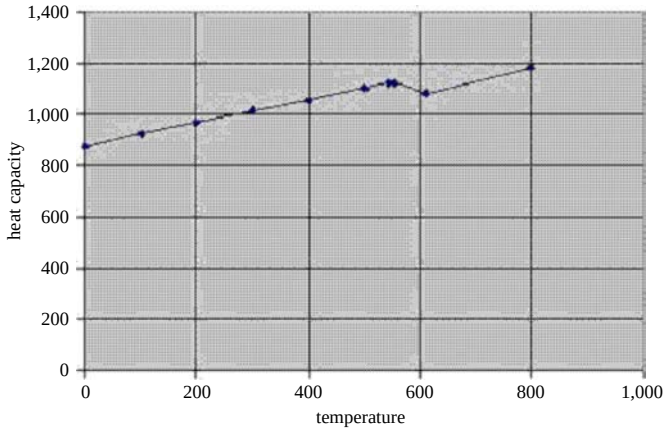

(a)

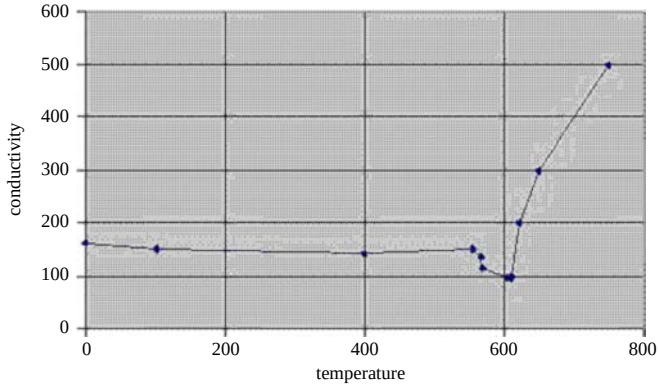

(b)

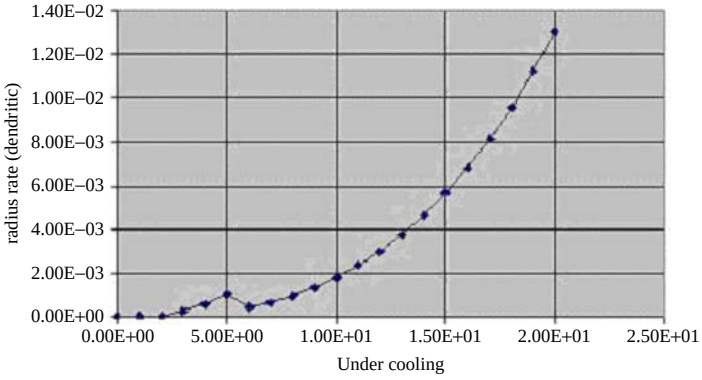

(c)

(Continued)

Figure 3.
Microstructural data (a, b, c, d): eutectic and dendritic radius rates with respect to undercooling, heat capacity and conductivity vs temperature

Note: Reproduced from the only available original

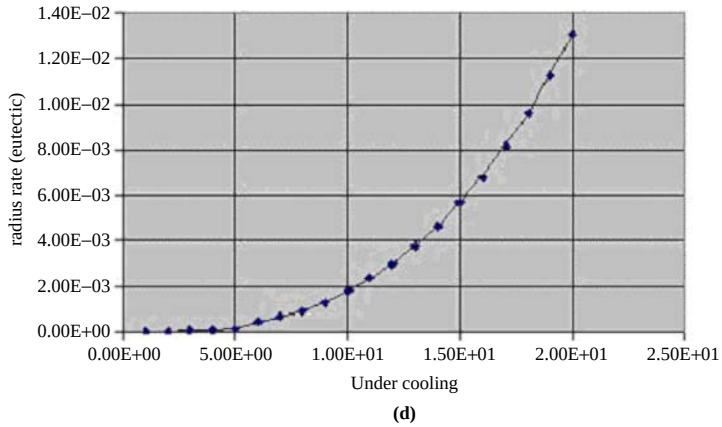

Note: Reproduced from the only available original

Figure 3

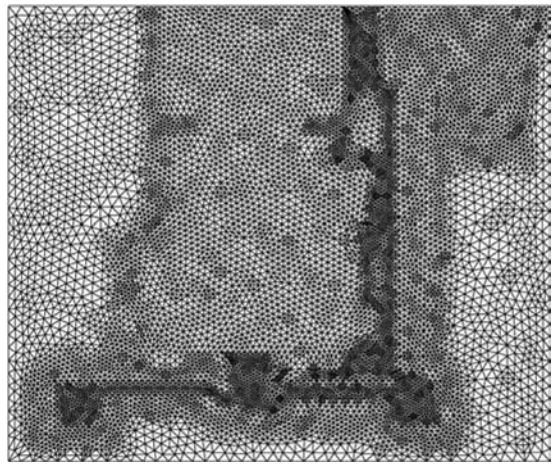

Figure 4.
Valve, finite element mesh

4.2 Coupling the mould filling and thermal stress analyses

In this case we follow the general assumptions that the process is sequential, which implies that the thermal stress analysis is performed after filling the mould with metal and reaching the final position of the punch. The latter implies that the final shape has been achieved. In this process the temperature field obtained at the end of the mould filling process represents the initial condition for the thermal stress transient analysis.

An example of an industrial squeeze forming process is described herein. Figures 12 and 13 show the coolant channel system of the punch and die. The problem is actually considered as axisymmetric, and the part being formed is a wheel. The material

Figure 5.
Valve, free solidification, temperature distribution

Note: Reproduced from the only available original

Figure 6.
Valve, free solidification, dendrite fraction distribution

Note: Reproduced from the only available original

properties are the same as presented in the previous examples. The diameter of the wheel is 0.5 m, the diameter of the die-punch-ring system is 0.9 m, the height of the punch is 0.23 m and the thickness of the part is 0.015 m. The initial temperatures of the particular parts of the system were as follows: cast 650° die and ring 280° and punch 300°. The enthalpy curves standing for the data are shown in Figure 14.

The sequence of the punch positions and the corresponding advancement of filling of the cavity by means of the distribution of the pseudo-concentration function is shown in Figures 15-20.

The maximum punch travel is 49 mm. The temperature distribution, after completion of the filling process, is shown in Figure 21. The next figure, Figure 22, shows the temperature distribution after 16 s of the cooling phase.

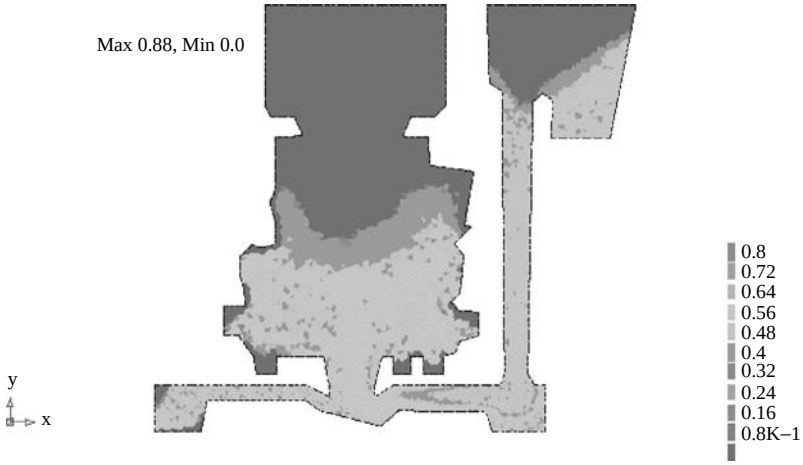

Note: Reproduced from the only available original

Figure 7.
Valve, free solidification, eutectic fraction distribution

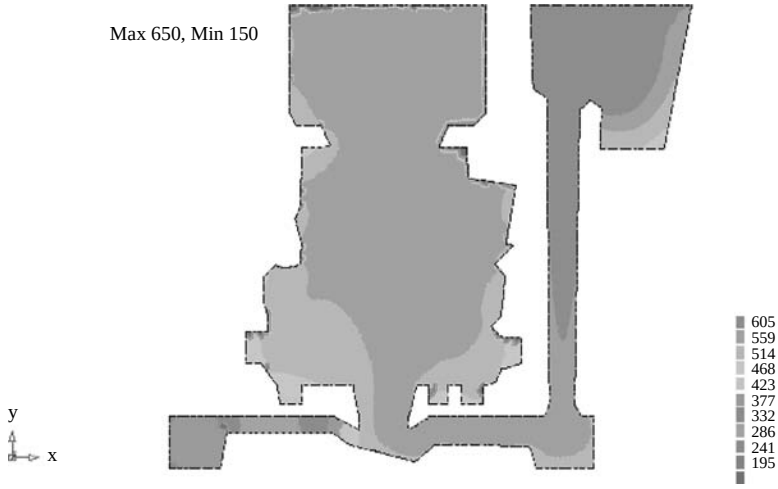

Note: Reproduced from the only available original

Figure 8.
Valve, squeezed casting, temperature distribution close to the end of the solidification process

The corresponding solidification pattern is shown in Figure 23 and the von Mises stress distribution is shown in Figure 24. The highest von Mises stress, 325 MPa, is in the punch close to the top of the cast part.

4.3 Parallel processing

4.3.1 Cylinder. The cooling process is calculated over a total time of 10 s. The diameter of the mould is 0.084 m, the diameter of the casting is 0.034 m, the height of the casting is 0.075 m and the height of the mould is 0.095 m, respectively. The following thermal boundary and initial conditions were assumed: a constant temperature of 20°C on the outer surface of the mould, 200°C on the top of the casting, 700°C being the initial

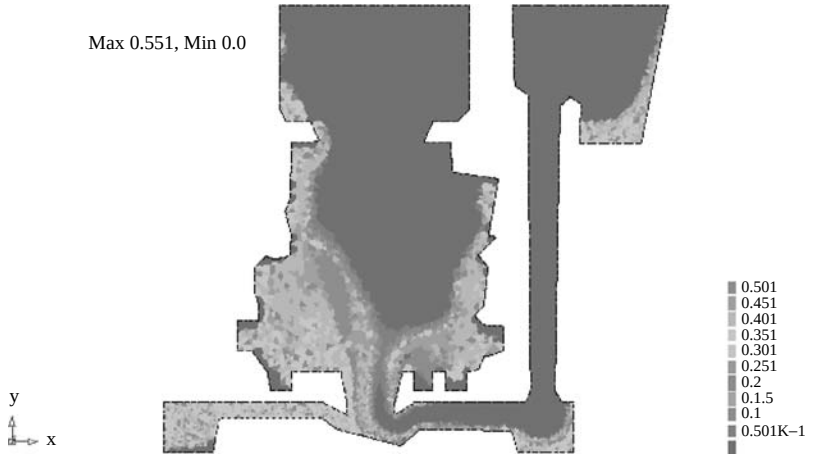

Note: Reproduced from the only available original

Figure 9.
Valve, squeezed casting, dendritic fraction distribution close to the end of the solidification process

Note: Reproduced from the only available original

Figure 10.
Valve, squeezed casting, eutectic fraction distribution close to the end of the solidification process

temperature of the casting and 200°C the initial temperature of the mould, respectively. The mould is fixed rigidly to the foundation. The die is made of steel H13 with the properties: Young modulus 0.25×10^{12} N/m^2, Poisson's ratio 0.3, density 7,721 kg/m^3, yield stress 0.55×10^{10} N/m^2, thermal exp. coeff. 0.12×10^{-5} and the material properties of the casting (aluminium alloy, LM25): Young modulus 0.71×10^{11} N/m^2, Poisson's ratio 0.3, density 2,520 kg/m^3, yield stress 0.15×10^{9} N/m^2, fluidity parameter 0.1×10^{-2}, thermal exp. coeff. 0.21×10^{-4}, contraction 0.3×10^{-12}, $T_{liq} = 612$°C, $T_{sol} = 532$°C. The enthalpy curves are shown in Figure 14.

The mesh (9,140 elements and 10,024 nodes), temperature, solidification ratio and Mises stress distributions at a time of 5 s are shown in Figures 25-28, respectively.

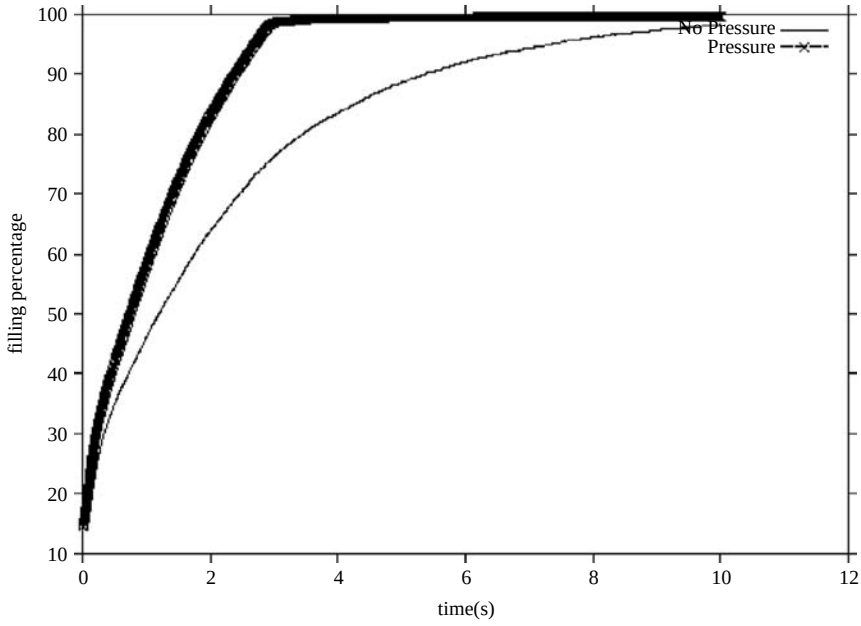

Note: Reproduced from the only available original

Figure 11.
Valve, dependence of the filling percentage versus time

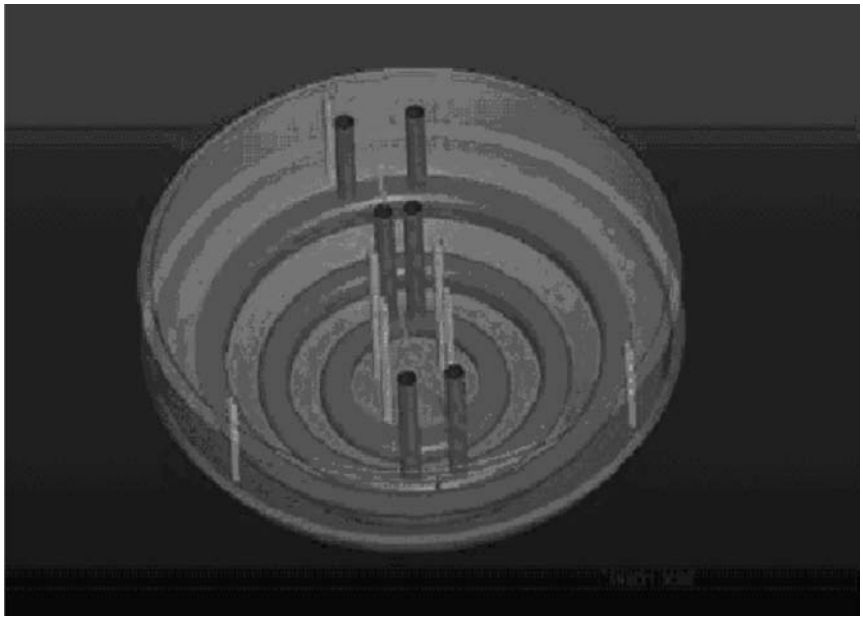

Note: Reproduced from the only available original

Figure 12.
Wheel, punch, coolant channel system

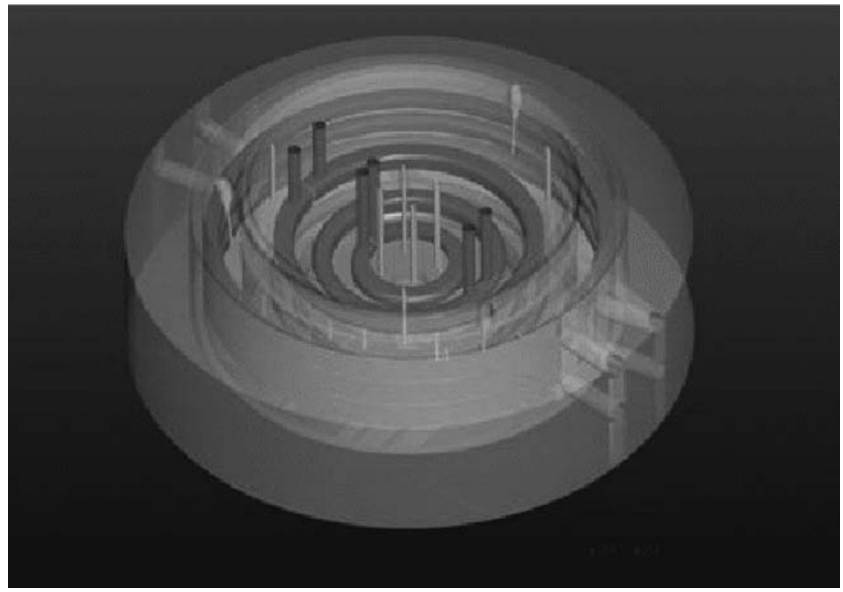

Figure 13.
Wheel, die, coolant channel system

Note: Reproduced from the only available original

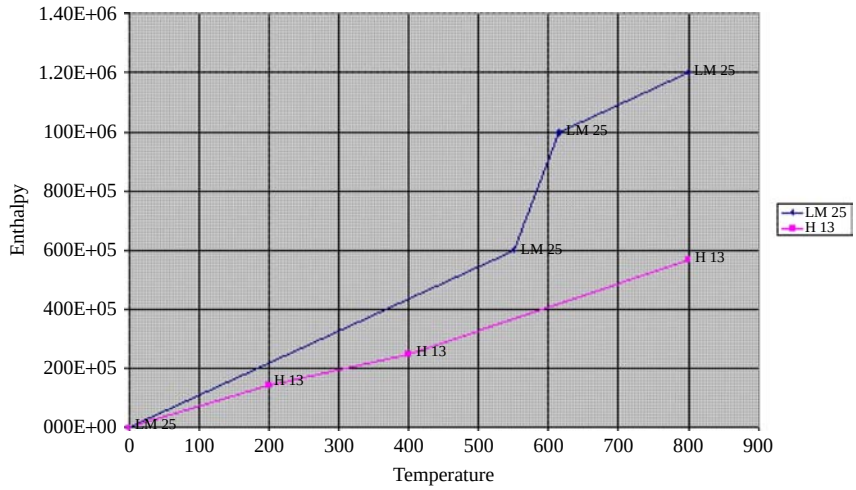

Figure 14.
Enthalpy curves used during the simulation

Note: Reproduced from the only available original

The program has been successfully tested on a range of 2-16 CPUs. The timing results, depending on the number of CPUs, are shown in Table I.

The master CPU uses more time then the rest of the CPU's since it prepares the stiffness matrices, right-hand sides of both problems and also takes part in the solution of the system of equations. The triangularization times for the thermal and mechanical

Note: Reproduced from the only available original

Figure 15.
Punch-die-cast system, position of the punch − 1 mm

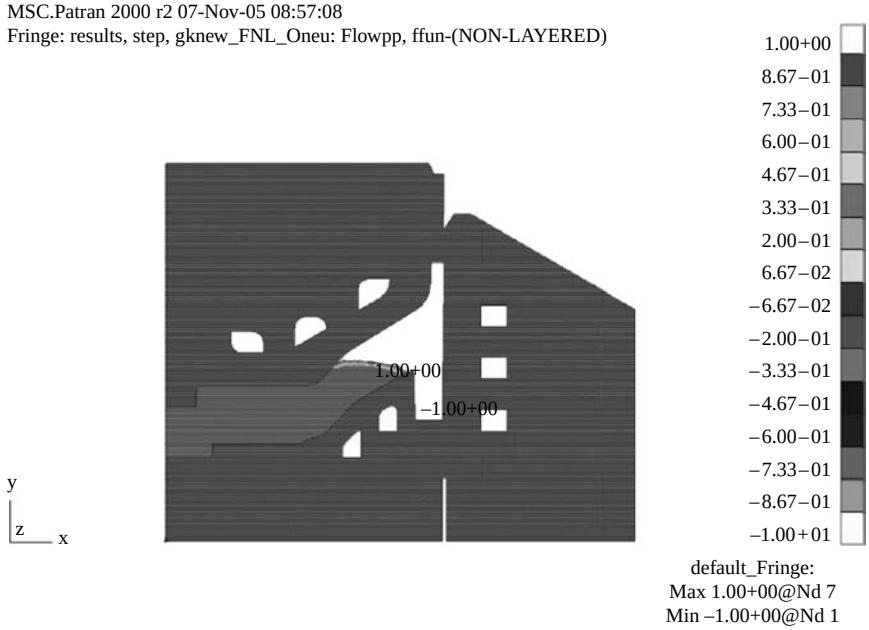

Note: Reproduced from the only available original

Figure 16.
Punch-die-cast system, position of the punch − 10 mm

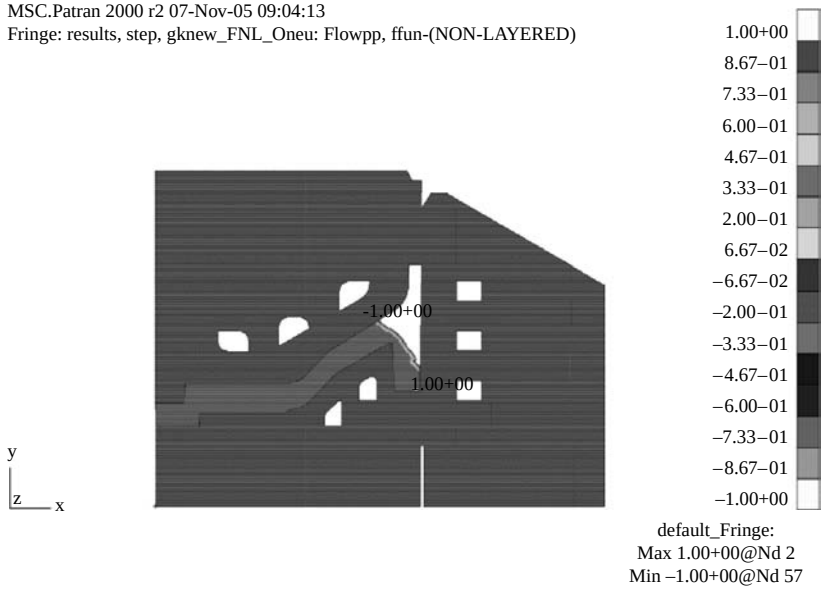

Figure 17.
Punch-die-cast system, position of the punch, −35 mm

Note: Reproduced from the only available original

Figure 18.
Punch-die-cast system, position of the punch, −40 mm

Note: Reproduced from the only available original

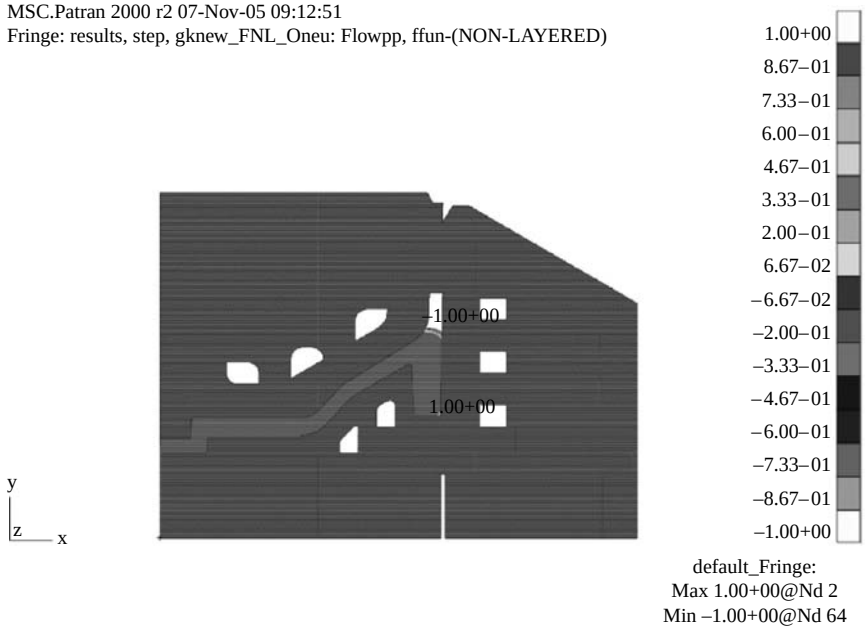

Note: Reproduced from the only available original

Figure 19.
Punch-die-cast system, position of the punch, – 45 mm

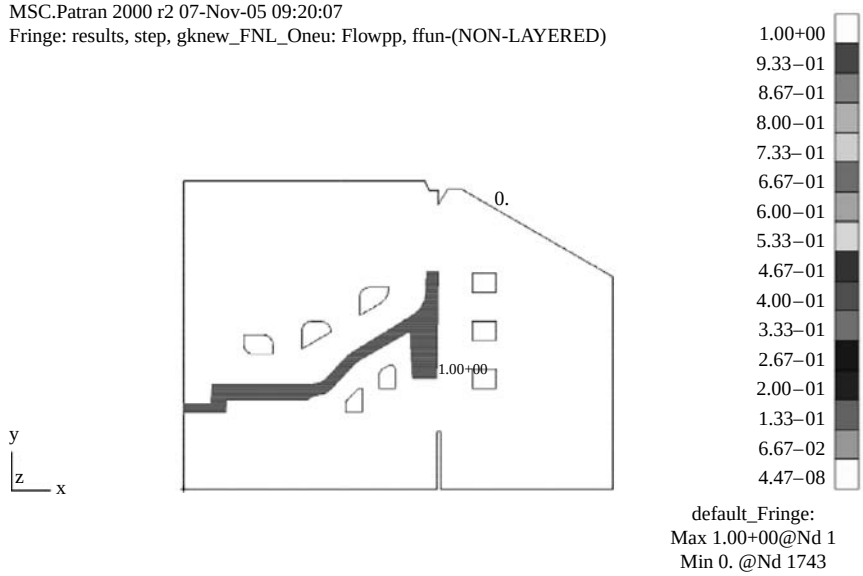

Note: Reproduced from the only available original

Figure 20.
Punch-die-cast system, position of the punch, – 49 mm

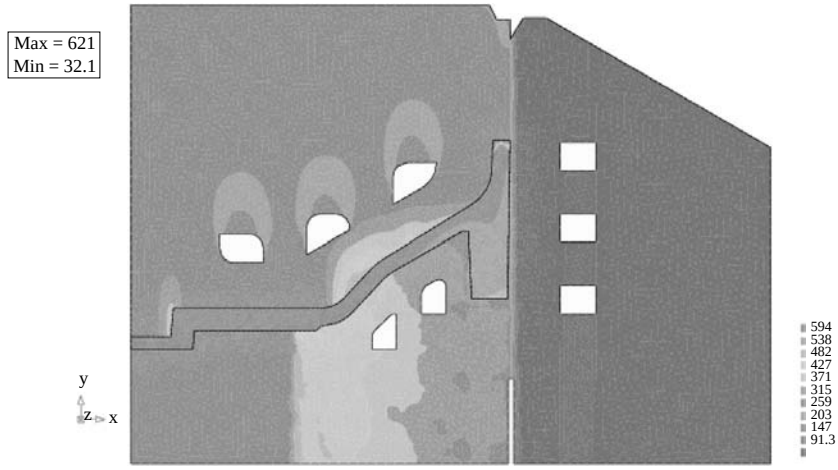

Note: Reproduced from the only available original

Figure 21.
Temperature distribution after completing of the filling phase

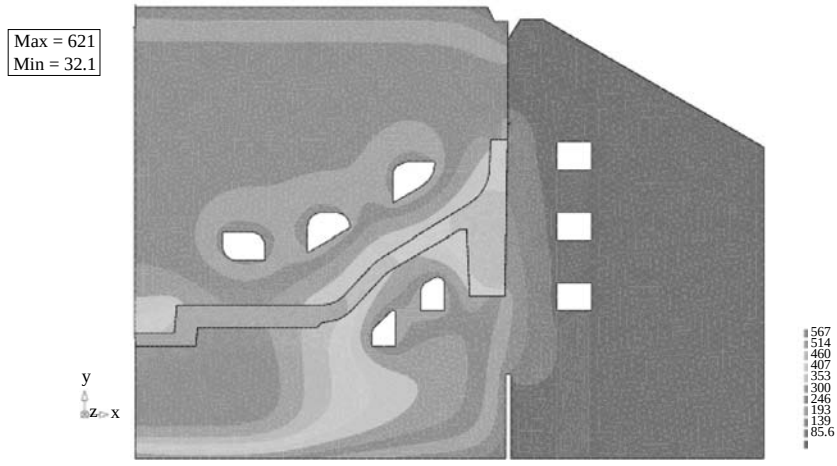

Note: Reproduced from the only available original

Figure 22.
Temperature distribution at 16 s of the cooling phase

problems are also different as the mechanical problem has three times the number of unknowns than the thermal problem.

The total times used by the master and slave processors, depending on their number, are given in Table I. An almost linear dependency of the total times used by the processors is demonstrated. The triangularization times are also given in Table I.

The acceleration factors and efficacies of the master and slave processors, depending on their number, are given in Table II.

The factors are referred to a base number of 2 CPU's.

On considering the thermomechanical problems it appears that the mean efficiency of the slave processor is higher than the master one. Indeed, the master processor

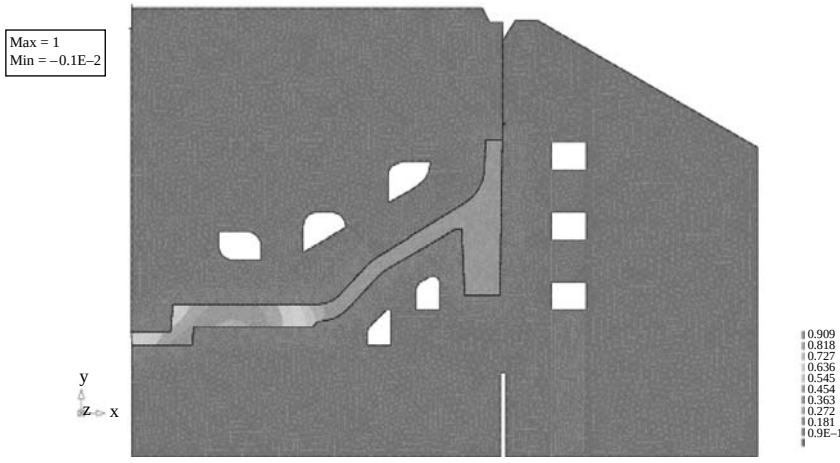

Note: Reproduced from the only available original

Figure 23.
Solidification ratio distribution, 16 s of the cooling

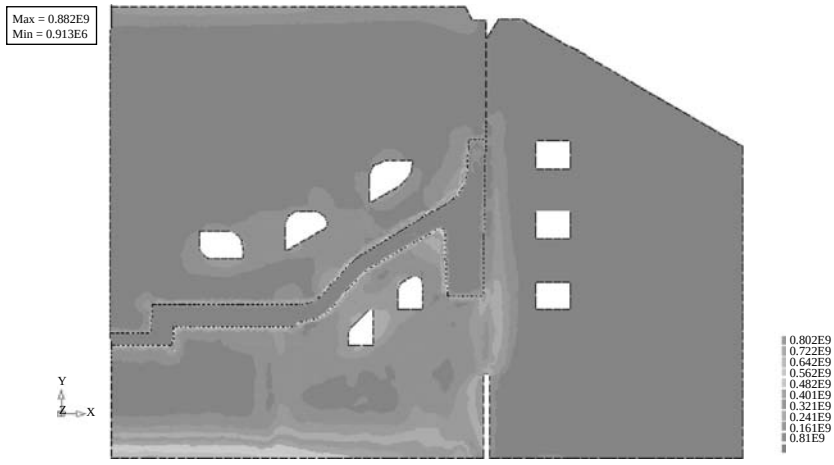

Note: Reproduced from the only available original

Figure 24.
Von Mises stress distribution, 16 s of the cooling

builds at each time step the stiffness matrix and the right-hand side vector for the thermal and mechanical modules. Also, the MUMPS software constructs at each time step a partition into N subdomains.

4.3.2 Aluminium part. This system consists of die with coolant channels, cylindrical cast and punch. The cylindrical cast has an opening. The geometry and the discretization are shown in Figure 29 (overall view) and in Figure 30 (cross-section). The physical properties are defined as in the example presented above. The system consists of 37,437 nodes and 33,920 elements.

The cooling process is followed for 5 s with 50 equal time steps and was solved using 16 CPUs. The solution required 13,271 s on the master CPU and 5,973 s of the remaining CPU's.

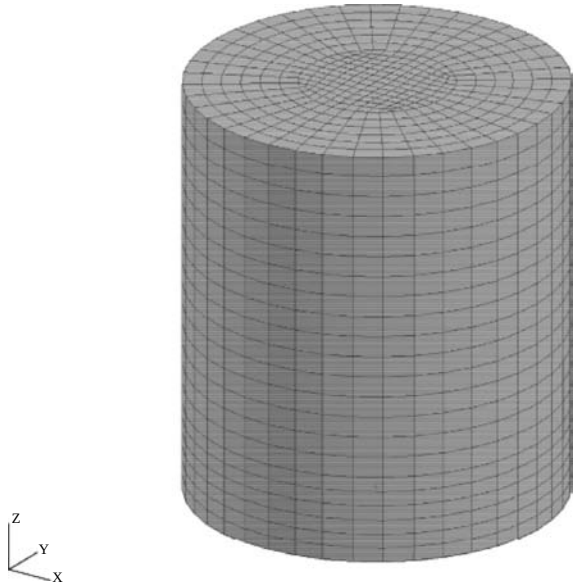

Figure 25.
Cylinder, finite element mesh

Note: Reproduced from the only available original

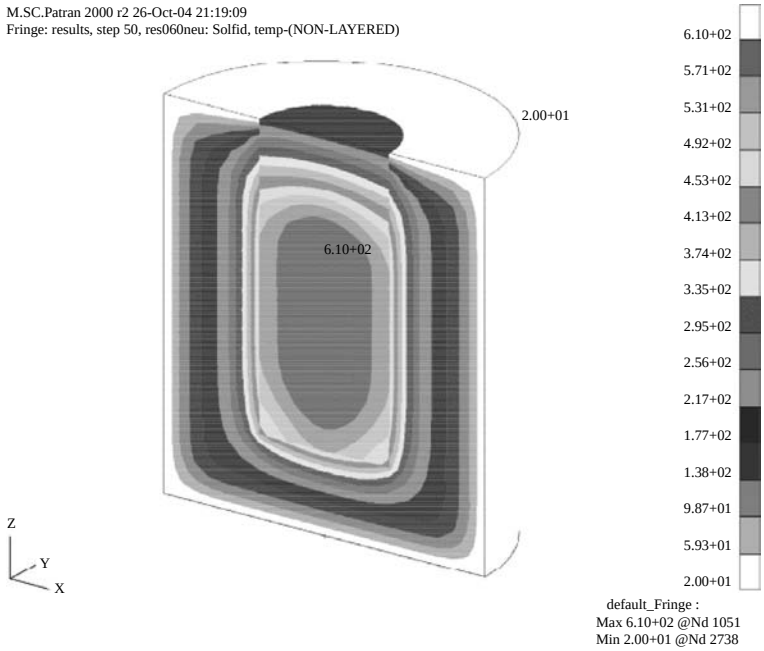

Figure 26.
Cylinder, temperature distribution, 5 s of the process

Note: Reproduced from the only available original

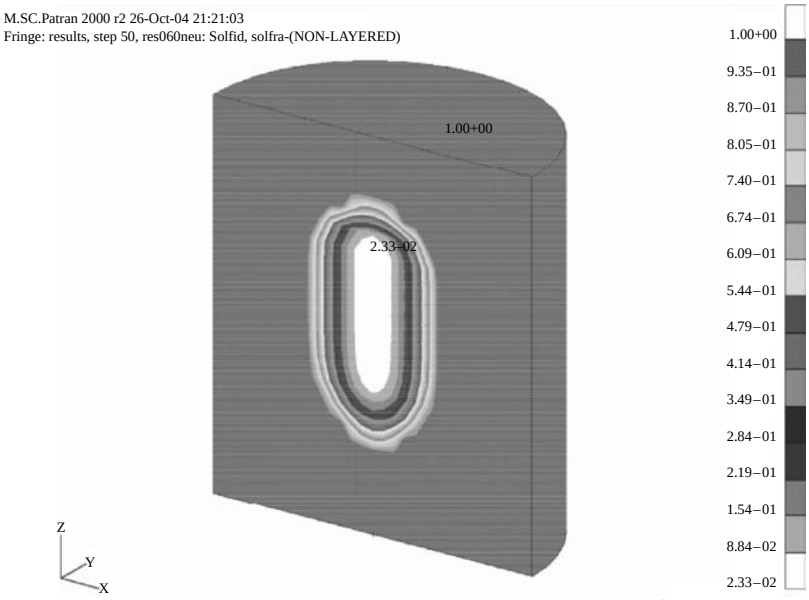

Figure 27.
Cylinder, solidification ratio, 5 s of the process

Note: Reproduced from the only available original

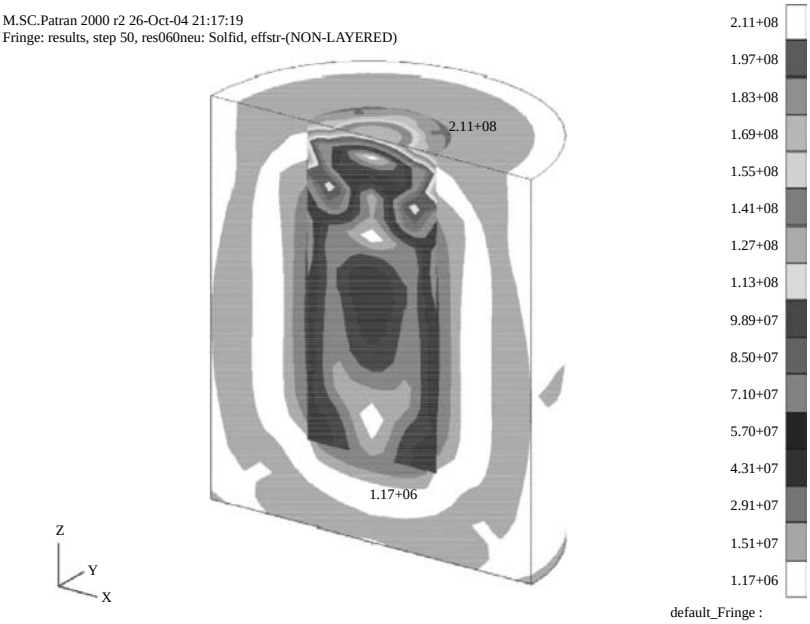

Figure 28.
Cylinder, solidification ratio, 5 s of the process

Note: Reproduced from the only available original

The distribution of temperatures is shown in Figure 30 and the distribution of the Mises stress is shown in Figure 31. We may notice that during the initial phase of the process the Mises stress are the highest in on the boundary between the cast and the die.

5. Final remarks

This paper presented a mathematical and computational framework of the squeeze forming process. We believe that further research, except for the usual refining of the present techniques, for example taking into account the effect of development of the thermal stresses during the filling phase, should be directed towards an analysis

Table I.
Timing of the problem (seconds)

No. of CPUs	Master CPU	Slave CPU	Triangularization time, thermal	Triangularization time, mechanical
2	8,294	6,797	0.8552	30.2115
4	6,193	4,682	0.5884	19.1354
8	3,084	1,898	0.2766	7.9217
16	2,296	2,296	0.1876	3.7895

Table II.
Acceleration and efficacy of the master CPU and slave CPUs

No. of CPUs	Master CPU Acceleration	Master CPU Efficacy	Slave CPU Acceleration	Slave CPU Efficacy
2	1.0	1.0	1.0	1.0
4	1.34	0.67	1.45	0.73
8	2.69	0.67	3.58	0.90
16	3.61	0.45	6.15	0.77

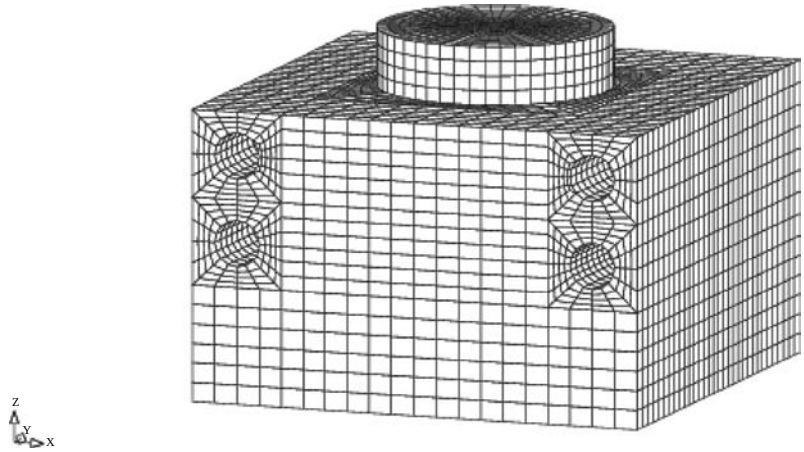

Figure 29.
Die-punch-cast setup

Note: Reproduced from the only available original

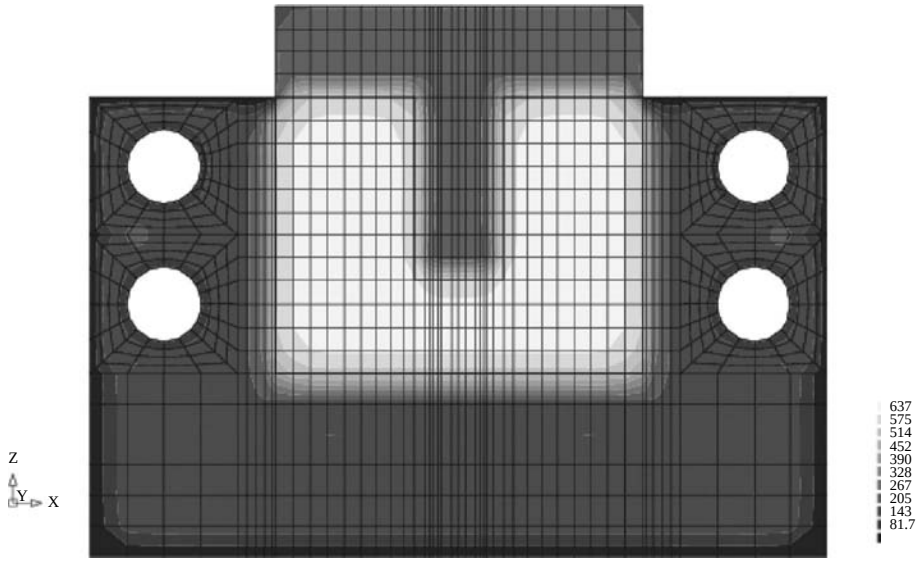

Figure 30.
Temperature distribution after 5 s of the process

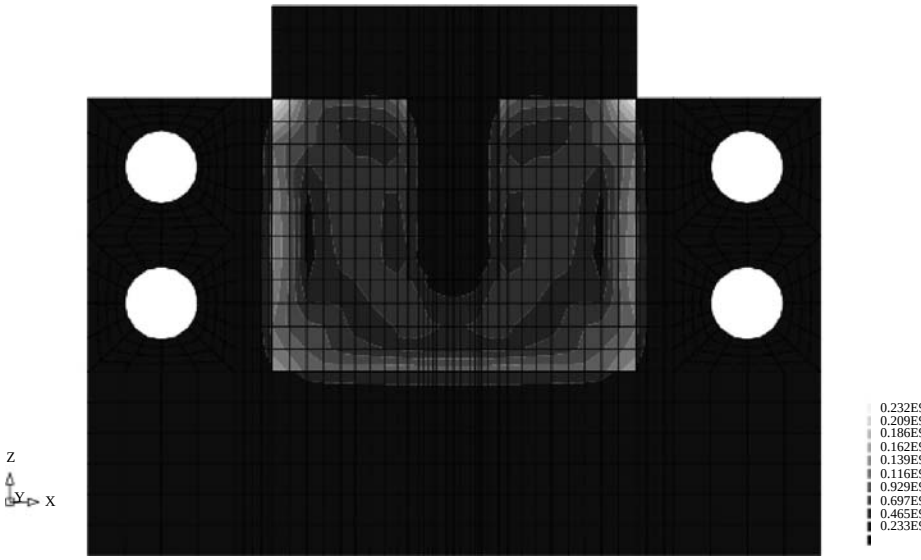

Figure 31.
Von Mises stress distribution, 5 s of the process

of the influence of geometrical defects (voids) in the parts, "artificial" inclusions, e.g. concentrations of eutectic or dendritic fractions, "hot spots" analysis, etc. This should lead to an evaluation of the reliability of the process. The reliability of the process is understood not only in its heuristic connotation but also as mathematically posed design constraints problem, i.e. reliability analysis.

References

Amestoy, P.R., Duff, I.S. and L'Excellent, J.Y. (2000), "Multifrontal parallel distributed symmetric and unsymmetric solvers", *Computer Methods in Applied Mechanics and Engineering*, Vol. 184, pp. 501-20.

Amestoy, P.R., Duff, L.S., Koster, J. and L'Excellent, J.Y. (2001), "A fully asynchronous multifrontal solver using distributed dynamic scheduling", *SIAM Journal of Matrix Analysis and Applications*, Vol. 23, pp. 15-141.

Bathe, K.J. (1996), *Finite Element Procedures*, Prentice-Hall, Englewood Cliffs, NJ.

Celentano, D.J. (2002), "A thermomechanical model with microstructure evolution for aluminium alloy casting processes", *International Journal of Plasticity*, Vol. 18 No. 10, pp. 1291-335.

Celentano, D. and Perez, E. (1996), "A finite element enthalpy technique for solving coupled nonlinear heat conduction/mass diffusion problems with phase change", *International Journal of Numerical Methods for Heat & Fluid Flow*, Vol. 6 No. 8, pp. 71-9.

Crisfield, M.A. (1997), *Non-linear Finite Element Analysis of Solids and Structures: Advanced Topics*, Wiley, New York, NY.

Donea, A. and Huerta, J. (2003), *Finite Element Methods for Flow Problems*, Wiley, New York, NY.

Felippa, C.A. and Park, K.C. (1980), "Staggered transient analysis procedures for coupled dynamic systems", *Computer Methods in Applied Mechanics and Engineering*, Vol. 26 No. 1, pp. 61-112.

Forum, MPI (1994), *MPI: A Message-Passing Interface Standard*, Technical Report, University of Tennesse, Knoxville, TN.

Ghomashchi, M.R. and Vikhrov, A. (2000), "Squeeze casting: an overview", *Journal of Materials Processing Technology*, Vol. 101 Nos 1/2, pp. 1-9.

Karypis, G. and Kumar, V. (1997), "METIS: A software package for partitioning unstructured graphs, partitioning meshes, and computing fill-reducing orderings of sparse matrices", Technical Report, University of Minnesota, Rochester, MN.

Kleiber, M. (1989), *Incremental Finite Element Modelling in Non-linear Solid Mechanics*, Polish Scientific Publishers, Ellis Horwood.

Kleiber, M. (1993), "Computational coupled non-associative thermo-plasticity", *Computer Methods in Applied Mechanics and Engineering*, Vol. 90 Nos 1/3, pp. 943-67.

Lewis, R.W. and Ransing, R.S. (1998), "A correlation to describe interfacial heat transfer during solidification simulation and its use in the optimal feeding design of castings", *Metallurgical and Material Transactions B*, Vol. 29 No. 2, pp. 437-8.

Lewis, R.W. and Ravindran, K. (2000), "Finite element simulation of metal casting", *International Journal for Numerical Methods in Engineering*, Vol. 47 Nos 1/3, pp. 29-59.

Lewis, R.W., Navti, S.E. and Taylor, C. (1997), "A mixed Lagrangian-Eulerian approach to modelling fluid flow during mould filling", *International Journal for Numerical Methods in Fluids*, Vol. 25 No. 8, pp. 931-52.

Lewis, R.W., Nithiarasu, P. and Seetharamu, K. (2004), *Fundamentals of the Finite Element Method for Heat and Fluid Flow*, Wiley, New York, NY.

Lewis, R.W., Morgan, K., Thomas, H.R. and Seetharamu, K. (1996), *The Finite Element Method in Heat Transfer Analysis*, Wiley, New York, NY.

Lewis, R.W., Postek, E.W., Han, Z.Q. and Gethin, D.T. (2006), "A finite element model of the squeeze casting process", *International Journal of Numerical Methods for Heat & Fluid Flow*, Vol. 16 No. 5, pp. 539-72.

McAdie, R.L., Cross, J.T., Lewis, R.W. and Gethin, D.T. (1995), "A finite element enthalpy technique for solving coupled nonlinear heat conduction/mass diffusion problems with phase change", *International Journal of Numerical Methods for Heat & Fluid Flow*, Vol. 5 No. 10, pp. 907-21.

Malvern, L.E. (1969), *Introduction to the Mechanics of Continuous Medium*, Prentice-Hall, Englewood Cliffs, NJ.

Masters, I., Usmani, A.S., Cross, J.T. and Lewis, R.W. (1997), "Finite element analysis of solidification using object-oriented and parallel techniques", *International Journal for Numerical Methods in Engineering*, Vol. 40 No. 15, pp. 2891-909.

Morgan, K., Lewis, R.W. and Zienkiewicz, O.C. (1978), "An improved algorithm for heat conduction problems with phase change", *International Journal for Numerical Methods in Engineering*, Vol. 12, pp. 1191-5.

Peric, D., Owen, D.R.J. and Honnor, M.E. (1992), "A model for finite strain elasto-plasticity based on logarithmic strains: computational issues", *Computer Methods in Applied Mechanics and Engineering*, Vol. 94 No. 1, pp. 35-61.

Postek, E.W., Denis, C., Jezequel, F., Lewis, R.W., Gethin, D.T. and Grima, N. (2005) A Concept of Parallelization of a 3D FEM Thermomechanical Code, Presentation during HPC Europa Project Meeting, Edinburgh, UK, September.

Ransing, R.S., Lewis, R.W. and Gethin, D.T. (1999), "Lewis-Ransing correlation to optimally design the metal-mould heat transfer", *International Journal of Numerical Methods for Heat & Fluid Flow*, Vol. 9 No. 3, pp. 318-32.

Ravindran, K. and Lewis, R.W. (1998), "Finite element modelling of solidification effects in mould filling", *Finite Elements in Analysis and Design*, Vol. 31 No. 2, pp. 99-116.

Simo, J.C. and Taylor, R.L. (1985), "Consistent tangent operators for rate independent elastoplasticity", *Computer Methods in Applied Mechanics and Engineering*, Vol. 48 No. 1, pp. 101-18.

Sluzalec, A. (1992), *Introduction to Nonlinear Thermomechanics*, Springer, Berlin.

Taylor, C. and Hughes, T.G. (1981), *Finite Element Programming of the Navier Stokes Equations*, Pineridge, Swansea.

Vaz, M. and Owen, D.R.J. (1996), *Thermo-mechanical Coupling: Models, Strategies and Application CR/945/96*, University of Wales Swansea, Swansea.

Williams, J.R., Lewis, R.W. and Morgan, K. (1979), "An elasto-viscoplastic thermal stress model with applications to the continuous casting of metals", *International Journal for Numerical Methods in Engineering*, Vol. 14 No. 1, pp. 1-9.

Zienkiewicz, O.C. and Taylor, R.L. (2005), *The Finite Element Method*, 6th ed., Butterworth-Heinemann, Oxford.

Zienkiewicz, O.C., Taylor, R.L. and Nithiarasu, P. (2005), *The Finite Element Method for Fluid Dynamics*, 6th ed., Elsevier, Amsterdam, p. 435.

Further reading

Crisfield, M.A. (1991), *Non-linear Finite Element Analysis of Solids and Structures*, Wiley, New York, NY.

Corresponding author

Eligiusz W. Postek can be contacted at: earewp@earth.leeds.ac.uk